Criticality and pattern formation in fracture by residual stresses

Kwan-tai Leung*
Institute of Physics, Academia Sinica, Taipei 11529, Taiwan, Republic of China and Graduate Institute of Biophysics, Department of Physics, National Central University, Jhongli 32054, Taiwan, Republic of China

Zoltán Néda†
Department of Theoretical Physics, Babeş-Bolyai University, Street Kogalniceanu, Number 1, RO-3400 Cluj-Napoca, Romania
(Received 13 August 2010; revised manuscript received 24 September 2010; published 26 October 2010)

We address the slow generation of crack networks as a problem of pattern formation. Issues of pattern selection and the associated statistical properties were considered by means of a detailed theoretical analysis and simulations of a discrete spring-block model. Developed after observations in desiccation experiments, the model describes the nucleation and propagation of cracks in a layer in contact with a frictional substrate. Competition between stress concentration at crack tips and pinning effect by friction leads to a cellular pattern. We characterized the events prior to cracking by a growth of correlation in the stress field, and those during cracking by progressive damages manifested in the number of broken bonds and energy releases. Qualitatively distinct regimes were shown to correspond to different stages of development. A host of scaling behaviors in measurable quantities were derived and verified. In particular, consistent with experiments, fragment area was found to be quadratic in the layer thickness and be smaller with increasing friction, which explains why morphologically similar patterns may occur over a diverse length scales.

DOI: 10.1103/PhysRevE.82.046118 PACS number(s): 62.20.mt, 05.65.+b, 89.75.Fb, 46.50.+a

I. INTRODUCTION

Nature offers a rich variety of fascinating patterns [1]. Examples in snowflakes, surface features of living things, waves, and vortices in fluid spring to mind. As manifestations of the underlying physical processes, those patterns have inspired the studies of crystal growth [2], reaction-diffusive systems [3], and instabilities in fluids [4]. Another ubiquitous but relatively less explored example lies in the fracture of solids [5], as seen in cracked paintings, battered roads and dried out fields. Focusing on the crack patterns in a layer attached to a substrate, there are some early observations [1,6,7] but systematic studies are all fairly recent. There have been several experimental studies on colloidal and granular systems [8–14]. Theoretically, while it is quite intuitive when and how things break [15], a satisfactory mathematical account remains formidable [16] even for one crack propagating in a homogeneous medium [17]. The additional complexity arising from the interactions among many cracks [18] makes evolving networks even less tractable. Among others, two notable theoretical efforts were reported in Refs. [19,20].

There exists also a less mathematical approach based on the analogy with phase transitions [21,22]. Geometrically, crack patterns with similar characteristics occur over a wide range of scales from μm to km. This suggests some universal mechanism is at work. Universality implies the unimportance of microscopic details, so that the essential physics may be captured at the mesoscopic level. This view is supported by the parallel between the nucleation and propagation of a crack [23] to that of the nucleation and growth of droplets at first order phase transitions [24]. Thus, the problem consists of identifying the basic mechanism and the few important length and time scales. Along this line, several coarse-grained descriptions for crack networks have been studied to various levels of success [25–30]. In Ref. [29], we developed a discrete spring-block model to investigate the interplay between stick-slip and cracking. With a few control parameters, we characterized the basic pattern selection process. In this paper, we will report a thorough revisit of the model. Theoretical derivations or arguments will be given to strengthen the observations and numerical results reported in [29]. Overall, we will present a coherent picture for the role dissipation plays in the growth of correlation, the statistics of energy releases, and the resulting morphology of the network.

This paper is organized as follows. In the next section the model is defined. In Sec. III, theoretical and numerical results are presented in light of the temporal evolution of the crack network. To make this paper self-contained, some results in [29] will be recapitulated and extended in much greater details. Section IV contains our conclusion. Finally, the Appendix gives some mathematical details for the block slips.

II. BUNDLE-BLOCK MODEL

We consider the process of crack formation in a layer in contact with a frictional substrate. That may be caused by slow physical (e.g., embrittlement, contraction) and chemical (e.g., oxidation) changes in the properties of the layer, leading to various forms of failure [31], such as decohesion, buckling, spalling and in-plane cracking. In this paper, we will consider only the simplest kind, namely, in-plane cracking with the substrate undamaged in the process.

We identify the grain (which consists of a large number of atoms) in the layer as the basic unit relevant to crack forma-

*leungkt@phys.sinica.edu.tw
†zneda@phys.ubbcluj.ro

 ©2010 The American Physical Society

tion, and represent it as a block. The blocks are interconnected among nearest neighbors by bundles. Each bundle consists of H bonds (coil springs), and each bond has the same spring constant k, relaxed spring length l, and tensile breaking strength F_c. The elastic constant of an undamaged bundle is thus kH. The force needed to overcome friction (i.e., to slip a block), denoted by F_s, may be regarded as the breaking strength of the layer-substrate interface. In the case of slow fracture, the motion of a grain is overdamped by friction from the substrate. Thus, the system evolves in a quasistatic manner in which the buildup rate of stress is much slower than its relaxation rate. We take advantage of this property by using a threshold dynamics to update the configurations, as a cellular automaton, instead of solving the coupled set of differential equations of motion as done in molecular dynamics. The resulting model is simpler and computationally more efficient than an atomistic approach. Moreover, singularities and nonlinearities associated with crack tips are generated dynamically via the relaxation process so that no explicit truncation of the stress field is needed.

One feature of our model distinctive from conventional spring-block models is the use of bundles instead of ordinary springs. This is a trick to introduce the *effect* of the thickness of the sample without the overburden of three-dimensional computations. Thus, the parameter H should be regarded as an effective thickness parameter but not the thickness itself. It is a fair approximation if the evolution of the cracks is predominately in-plane. Physically, it applies to the case when the extent of elastic deformation is comparable to the thickness, and that the thickness is not considerably greater than the characteristic size of the ensuing pattern. Obviously, fracture dominated by varying material properties along the depth (such as in thick starch slurry [14]) calls for a full, three-dimensional treatment.

In the context of a drying experiment (see below), cracks are often caused by progressive changes in material properties, such as by the increase of hardness (i.e., k) and weakening of the breaking strengths (i.e., F_c within the layer, F_s to the substrate). Such changes lead to instabilities in the forms of block slips and bond breakages, depending on the ratio between the force and threshold. Since the ratio is proportional to k/F_s or k/F_c, we can model both hardening and weakening by keeping k constant and decreasing the thresholds in time. In general, the rates of change of the two thresholds are independent. For the case when both thresholds decrease at the same rate via the same physical change of material properties (such as hardening induced by the narrowing and breaking of liquid bridges between grains due to the evaporation of solvent in desiccation [13,14]), their ratio $\kappa \equiv F_c/F_s$ becomes a constant. In this paper, we will consider only that particular case [32]. One of the simplest conceivable way to induce fracture is then to prestrain the array and decrease slowly both F_s and F_c at the same rate. Even though this specification may not have an exact correspondence with experiments, it is physically related to the case of fracture by residual stresses. Other ways of driving are possible, but this is particularly simple to allow for some analytic understanding.

The blocks are labeled by (i,j) as shown in Fig. 1, where i runs from 1 to W, and j from 1 to $2L$. The configuration of

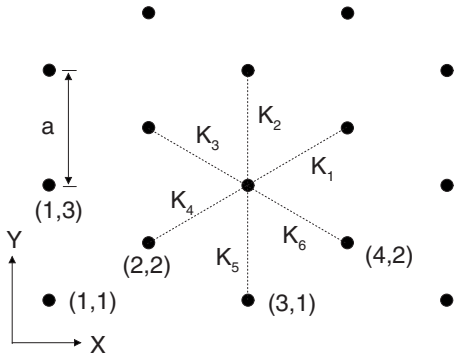

FIG. 1. The labeling of the blocks (i,j) and bonds K_i on a triangular lattice. a denotes the lattice spacing.

the system at any given time is defined by $3WL$ bundles [33] and the position vectors $\vec{R}_{i,j}$ of WL blocks. Each bundle has a certain number (between 0 and H) of unbroken bonds, and the position vectors are given by

$$\vec{R}_{i,j} = (X_{i,j}, Y_{i,j}) = (X^0_{i,j} + x_{i,j}, Y^0_{i,j} + y_{i,j}). \tag{1}$$

Here $\vec{R}^0_{i,j} \equiv (X^0_{i,j}, Y^0_{i,j})$ is the node of a triangular lattice of spacing a, and $\vec{r}_{i,j} \equiv (x_{i,j}, y_{i,j})$ denotes the random displacement, typically a few percents of a. The tensile prestrain is given by $s=(a-l)/a>0$. Generally, due to $\vec{r}$ the net force $\vec{F}$ exerted on a block by its neighbors is nonzero. In a stable configuration that force is balanced by friction.

With Hookean bonds, the force exerting on a given block at $\vec{R}_{i,j}$ by a neighboring block at $\vec{R}'$ is given by $(|\vec{R}_{i,j} - \vec{R}'| - l)kH$. However, this nonlinear dependence on the coordinates results in slow updating. Since the system cracks by tensile stress and that the prestrain $s \ll 1$, to a good approximation we may expand $\vec{F}$ to first order in $\vec{r}/a$. It is then straight forward to show that the force components on the block (i,j) are given by

$$F^x_{i,j} = k\sum_{n=1}^{6} H_n[asC_n + (x_n - x_{i,j})(sS_n^2 + C_n^2) + (y_n - y_{i,j})(1-s)S_nC_n], \tag{2}$$

$$F^y_{i,j} = k\sum_{n=1}^{6} H_n[asS_n + (y_n - y_{i,j})(sC_n^2 + S_n^2) + (x_n - x_{i,j})(1-s)C_nS_n], \tag{3}$$

where the index n labels the six nearest neighbors of the block (i,j) and its connecting bundles. H_n takes on a value between 0 and H, and the constants $C_n = \cos[(2n-1)\pi/6]$ and $S_n = \sin[(2n-1)\pi/6]$ arises from the symmetry of the triangular lattice. Note that these force components are signed variables, whereas the threshold conditions are based on absolute values.

Initially, the thresholds are set so high as to ensure global stability. In discrete simulation time steps labeled by t, the configuration evolves according to the following dynamical rules:

(1) The thresholds are lowered systematically until either the global maximum force or tension is reached from above. A marginally unstable block or bundle is located.

(2) If $F \equiv |\vec{F}| > F_s$, the block slips to its new mechanically equilibrium position where $F=0$.

(3) If the tension of the bonds in a bundle exceeds F_c, one of the bonds of that bundle is broken, i.e., $H \to H-1$ there, provided no more than one bond in that bundle is broken within the given simulation step.

(4). Iterate steps no. 2 and no. 3 for all affected blocks and bundles.

After a sequence of slippings and/or breakings [34], the system settles into a new metastable state. This completes one simulation step, and the next step follows $(t \to t+1)$. By limiting to one broken bond per bundle per step in no. 3, we attempt to model the progressive damage of bundles; otherwise unphysical vertically oriented "tunnel" may be spontaneously generated.

Although other dynamical rules are conceivable, the details of implementation is expected to be of secondary importance compared to the basic ingredients consisting of the stick-slip action and threshold dynamics. Not knowing the actual time dependence of system parameters in desiccation experiments, we inevitably have a certain degree of arbitrariness in the rules. In making our choices, we are guided by the balance of physical relevance, robustness in producing nontrivial patterns, as well as algorithmic simplicity. For instance, having two independent thresholds is equivalent to allowing κ to vary in time, which would lead to considerable complications in the analysis.

Note that rule no. 2 implies zero kinetic friction. If we introduce nonzero kinetic friction F_k with $0 < F_k < F_s$, a slipping block will be arrested before it reaches the zero-force position. We show in the Appendix that such a more general case only leads to a simple modification in the slipping distances, so that the general behaviors of the model are unchanged.

III. RESULTS AND DISCUSSIONS

We used square samples with linear size $W=L \leq 300$. Without loss of generality, we henceforth choose our units such that $a=1=k$. The forces and energies in the following equations are understood to have been rescaled properly. This leaves us a set of four control parameters $\{s, \kappa, H, L\}$. Since the strain in reality is quite small, we took $0 < s < 0.2$. We considered free boundary conditions (FBC), although periodic boundary conditions (PBC) had also been used for comparison [35].

Qualitatively, the time evolution can be divided into three phases:

(I) Prefracture phase: there are slippings only, bonds are too strong to be broken;

(II) Fracture phase: There are slippings and bond breakings, the system is progressively damaged and broken up into fragments which then contract slowly;

(III) Saturation phase: bond-breaking event saturates, fragmentation stops, slippings dominate again as the interblock spacing approaches the relaxed spring length l asymptotically.

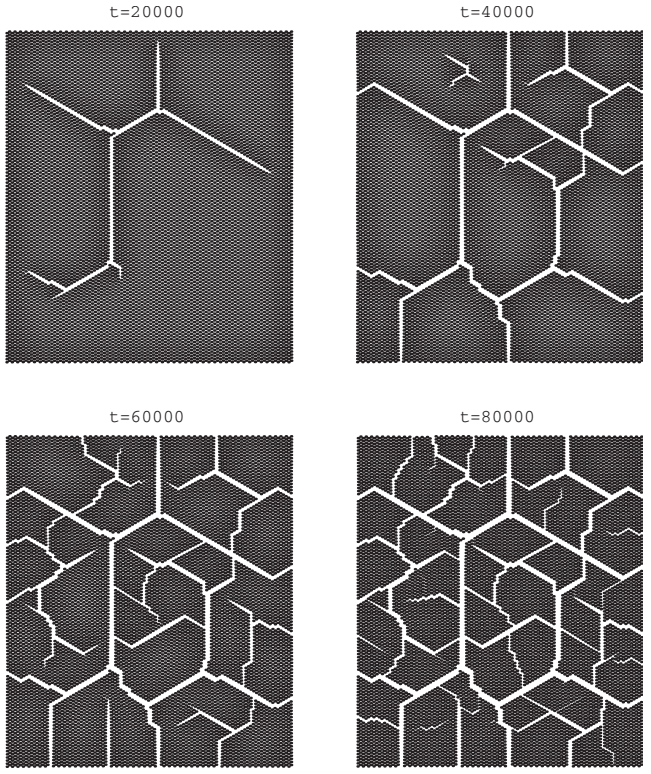

FIG. 2. Evolution at different simulation step t for $L=100$, $s=0.1$, $\kappa=0.5$, $H=9$, under FBC, showing the progressive change from straight to diffusive cracks.

Some typical configurations in phase II are shown in Fig. 2. We now discuss their characteristics following the temporal order of evolution.

A. Decrease of thresholds

We will examine the decrease of the thresholds first, for it is the driving force behind the evolution. In a stable configuration, each block is associated with a force F, where $0 \leq F < F_s$. Due to the dynamical rule no. 1 of Sec. I, the decay rate of F_s is inversely proportional to the density of state in the F variable close to F_s. In a mean-field approximation, this density is F_s/L^2. Hence $F_s(t)-F_s(t+1) \propto F_s(t)/L^2$, leading to $F_s(t) \propto e^{-t/\tau}$ [see Fig. 3(a)] with a decay constant $\tau \sim L^z$ and a mean-field exponent $z_{\mathrm{MF}}=2$. Numerically, we find $z=1.78 \pm 0.03$ [see Fig. 3(b)], reflecting the nonuniform distribution of the F values in the interval between 0 and F_s. This may be interpreted as a depletion effect of the population of F near F_s relative to a uniform distribution, by the avalanches of slippings.

Concerning the effect of thickness H, consider two identically prepared systems (with the same initial random positions of blocks) except having different H. Before cracking, the system evolves only by slippings. The slip distance for a block exerted by a force $F > F_s$ is given by $\delta r = F/H(3+3s)$ (see Appendix). Since $F \propto H$ (H being the elastic constant of undamaged bundles), δr is independent of H. This means the two systems have identical history (i.e., identical configurations at any given t) prior to cracking. Since slippings are

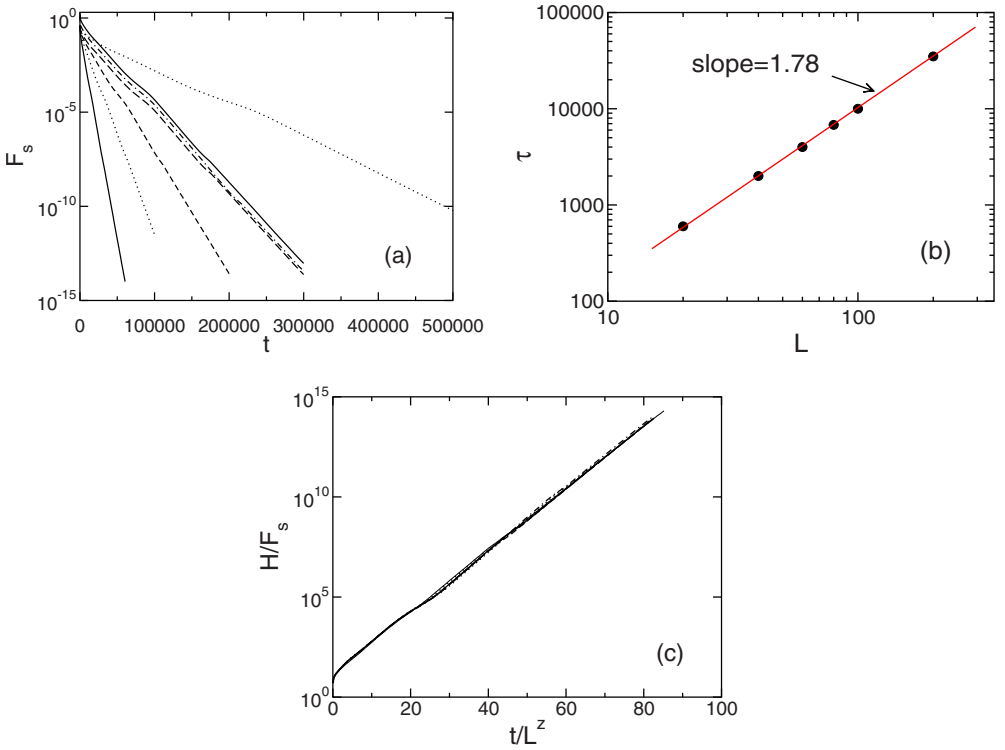

FIG. 3. (Color online) (a) Linear-log plot of the threshold vs simulation step, showing exponential decays $F_s \sim e^{-t/\tau}$. $s=0.1$, $\kappa=\infty$, and $H=2$ except stated otherwise, from left to right: $L=40$, 60, 80, 100, 100 ($H=4$), 100 ($H=8$), 160. (b) Decay constant extracted from (a) vs system size. Least-square fit gives an exponent $z=1.78\pm0.03$. (c) Scaling plot of the data in (a) for the threshold, with respect to thickness H, simulation step t and system size L.

determined by F/F_s, we must have $F_s \propto H$. Thus the system with larger H has slower decay in F_s,

$$F_s(t;H,L) = c_0 H e^{-t/\tau}, \tag{4}$$

$$\tau = c_1 L^z, \tag{5}$$

where c_0 and c_1 are constants, independent of H and L. Figure 3(c) confirms our derivation.

B. Growth of correlation before cracking

In phase I, the systematic release of elastic energy by slippings causes the system to contract and correlation to grow. Due to missing neighbors along free edges, slipping naturally starts there and invades into the bulk. The width ξ of the resulting strain-relieved peripheral region characterizes the extent of invasion. We now show that the growth of ξ is governed by the decay of the threshold. Evidently, the strain is small near the free boundaries, and it rises to the prestrain value s deep in the bulk (see Fig. 4). For simplicity, consider for the moment a one-dimensional version: the force exerted on the ith block by its two neighbors is given by $F_i=(a-l+x_{i+1}-x_i)H-(a-l+x_i-x_{i-1})H=(s_i-s_{i-1})aH$. Assuming smooth i dependence in x_i, we have $F \approx Hds/du$, where u is the distance from the edge. In the strain-relieved region, metastability imposes that $Hds/du \lesssim F_s$ (this does not apply beyond the invaded region where only $F<F_s$ can be assured). The rise of $s(u)$ from the edge is thus proportional to $F_s u/H$. This relation can obviously be extended to higher dimensions,

$$\xi(t) \approx \frac{\xi_0 s H}{2F_s(t)}, \tag{6}$$

where the constant ξ_0 is of order unity (factor 2 introduced for clarity in subsequent formulas). Thus, by Eq. (4), ξ grows exponentially in t. For a sufficiently small system of size L (explained below), ξ will saturate to $L/2$ when F_s reaches $F_s^{\rm sat}=\xi_0 H s/L$ at time

$$t_{\rm sat} = \tau \ln\left(\frac{c_0 H}{F_s^{\rm sat}}\right) = \tau \ln\left(\frac{c_0 L}{\xi_0 s}\right). \tag{7}$$

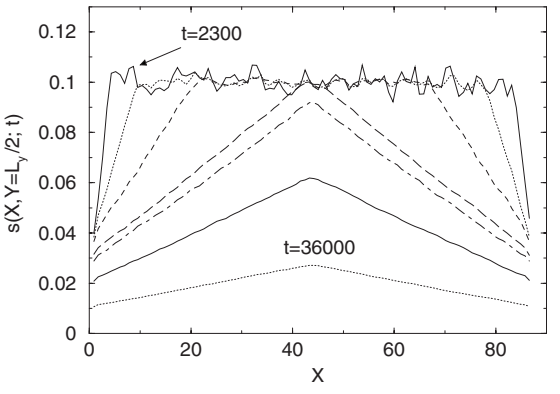

FIG. 4. Averaged strain field profiles showing progressive strain relief as simulation step t increases from 2300, 9200, 16 100, 22 500, 24 000, 28 000 to 36 000 for $L=100$, $s=0.1$, $H=2$, $\kappa=\infty$.

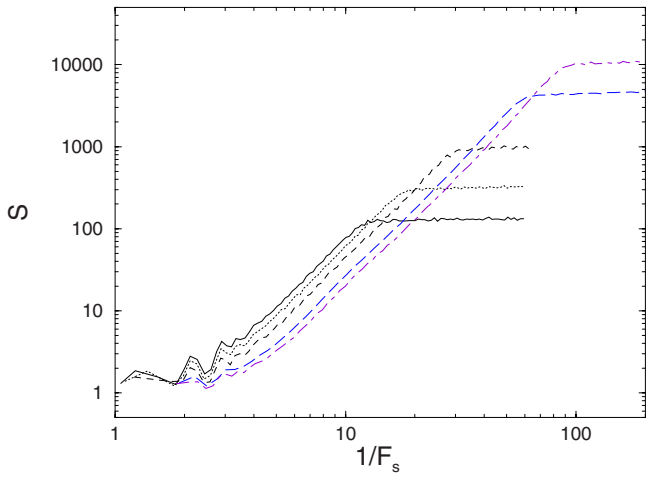

FIG. 5. (Color online) Power-law growth of the slip size vs the inverse threshold, $1/F_s$, which increases in time. $s=0.1$, $H=5$, $\kappa=\infty$, FBC, and system size $L=40$, 60, 100, 200, and 300 from left to right, with increasing level of saturation at long times.

Now we deduce the growth of slip size. In stick-slip models, the slip size $S(t)$, defined as the mean of the total number of block slips per simulation step, is often used to characterize the degree of correlation in the dynamical variable. It exhibits a power-law growth in time, followed by saturation (see Fig. 5). We may understand this behavior by energy balance as follows. The total energy relieved over the strain-relieved region, of the order $U=2\xi L s^2 H$, is dissipated by friction during slippings over that region. Since the slip distance is $\delta r=\alpha F/H$ (see Appendix), where $\alpha=1/3(1+s)$ [36], each slip dissipates an amount of energy $\alpha F_s^2/2H$. The total dissipation is then $E=\int_0^t dt' S(t')\alpha F_s(t')^2/2H$. Equating E to U and differentiating with respect to t, noting that $F_s(t) \sim He^{-t/\tau}$, we readily obtain the result

$$S(t) = S_0\left(\frac{H}{F_s(t)}\right)^3, \quad t < t_{\text{sat}}, \tag{8}$$

where the prefactor is $S_0=2\xi_0 s^3 L/\alpha\tau$.

These results have interesting finite-size effects. For $t < t_{\text{sat}}$, the invasion is unaware of the finite system size [apart from that through $F_s(t)$], hence ξ_0 is independent of L and so $S_0 \sim L^{1-z}$. For $t > t_{\text{sat}}$, as ξ saturates so does $S(t)$ to a constant

$$S_{\text{sat}} \equiv S(t_{\text{sat}}) = S_0\left(\frac{L}{s\xi_0}\right)^3 \sim L^{\eta}. \tag{9}$$

The divergence of S_{sat} as $L\to\infty$ means that the system becomes critical with a nontrivial critical exponent $\eta>0$ that is related to the "dynamic exponent" via a scaling relation

$$\eta = 4 - z. \tag{10}$$

From $z_{\text{MF}}=2$, we get $\eta_{\text{MF}}=2$. Simulations give $\eta=2.20\pm0.03$ instead (see Fig. 6), in agreement with the independent estimate of z. From Eq. (8), it is evident that dynamic scaling

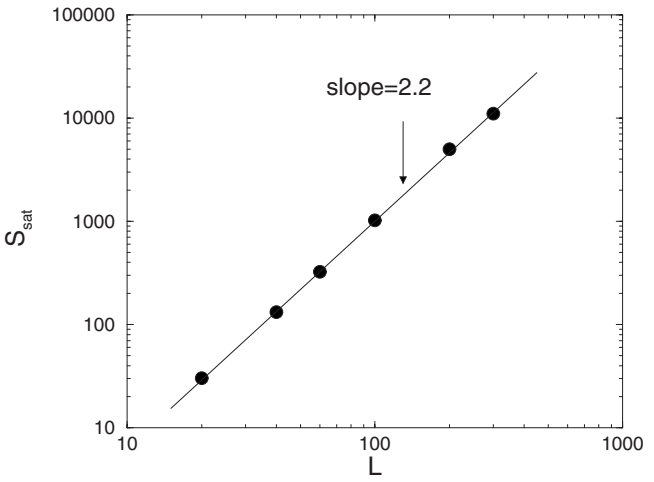

FIG. 6. Finite-size effect of the saturated slip size. The slope gives the exponent η in (9). $s=0.1$, $H=5$, $\kappa=\infty$, FBC.

$$S(t;H,L) = L^{\eta}\Phi\left(\frac{H}{LF_s(t)}\right) \tag{11}$$

is obeyed, with the scaling function $\Phi(x \ll 1) \sim x^3$ and $\Phi(x \gg 1)=\text{const}$, as exhibited in Fig. 7. This is the signature of a system approaching a self-organized critical (SOC) state [37] characterized by a power-law distribution of slip sizes.

For finite L and sufficiently large κ so that no bond can be broken at all (explained below), the correlation covers the entire system after time t_{sat}. The SOC state reached in this limit of large κ has been studied at length elsewhere [38], so we will not elaborate any further. On the other hand, for large enough L and small enough κ, fracture eventually sets in before criticality is fully attained. The system then goes through phase II and III as described above until it reaches a stationary fragmented state. Then, each fragment attains the very same critical state but with an individual cutoff limited by its own fragment size.

Before we move on, several remarks are in order:

(1) On the average, each site slips $L^{\eta-2}$ times per event after saturation. Since $\eta>2$, the computation becomes very

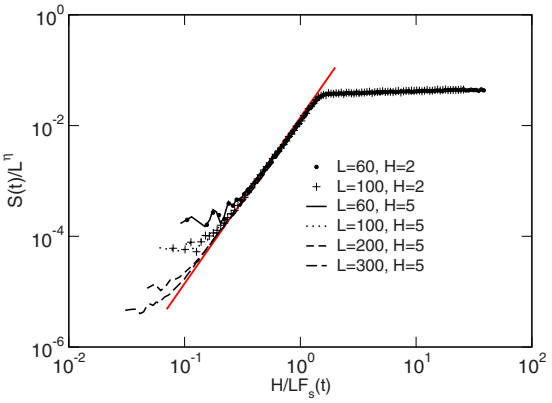

FIG. 7. (Color online) Dynamic finite-size scaling of mean slip size toward criticality. $s=0.1$, $\kappa=\infty$, $\eta=2.2\pm0.03$. The straight line has a slope equal to 3.

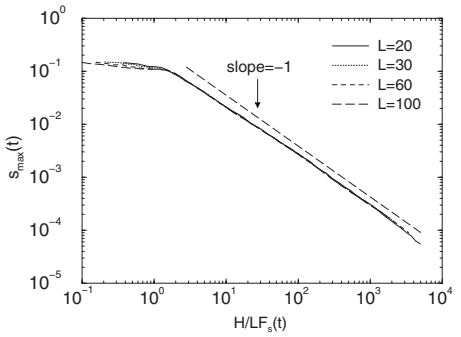

FIG. 8. Temporal variation of the maximum strain: $s_{\max}=s$ for $t<t_{\rm sat}$ and decays linearly in H/LF_s afterward. $s=0.1$, $H=2$, $\kappa=\infty$, various system sizes.

demanding for large system sizes. Such repeated topplings are manifestations of system-wide correlation in the force variable that controls the slippings.

(2) Since the connection between the dynamics (z) and criticality (η) is derived from a general energy argument, we speculate that relations similar to Eq. (10) should exist for other forms of driving and boundary conditions.

(3) Since subsequent fracture events depend on the maximally strained bonds, it is useful to find out how the global maximum strain $s_{\max}$ in the system behaves. Using Eq. (6), we find (see Fig. 8),

$$s_{\max} \approx \begin{cases} s & t < t_{\rm sat} \\ \dfrac{LF_s}{\xi_0 H} & t > t_{\rm sat}. \end{cases} \tag{12}$$

(4) Note that the parameter F_c, or κ, is irrelevant to the evolution of the system in phase I, but it governs the subsequent cracking process.

C. Onset of cracking

If F_c does not drop fast enough to get below s before time $t_{\rm sat}$, i.e., if $\kappa F_s^{\rm sat}=\xi_0\kappa Hs/L>s$ or $\xi_0\kappa H>L$, Eq. (12) shows that $s_{\max}$ will remain smaller than κF_s for all $t>t_{\rm sat}$, and the system will not crack. It cracks only if F_c catches up with s at some time $t^*<t_{\rm sat}$ as determined by

$$F_s^* \equiv F_s(t^*) \approx \frac{s}{\kappa}. \tag{13}$$

Using Eq. (4), we obtain the time of onset

$$t^* \approx \tau \ln\left(\frac{c_0\kappa H}{s}\right) = t_{\rm sat} - \tau \ln\left(\frac{L}{\xi_0\kappa H}\right). \tag{14}$$

Since Eq. (14) applies only to the case of $L>\xi_0\kappa H$, we get $t^*<t_{\rm sat}$, i.e., that cracking always happens before the saturation of correlation if it does happen. The scaling behavior of t^* is confirmed in Fig. 9.

Equation (14) shows that a system with a larger H takes a longer time to crack by the factor $\ln H$. This gives rise to more slippings and longer correlation at the onset,

$$S^* \equiv S(t^*) = S_0\left(\frac{\kappa H}{s}\right)^3, \tag{15}$$

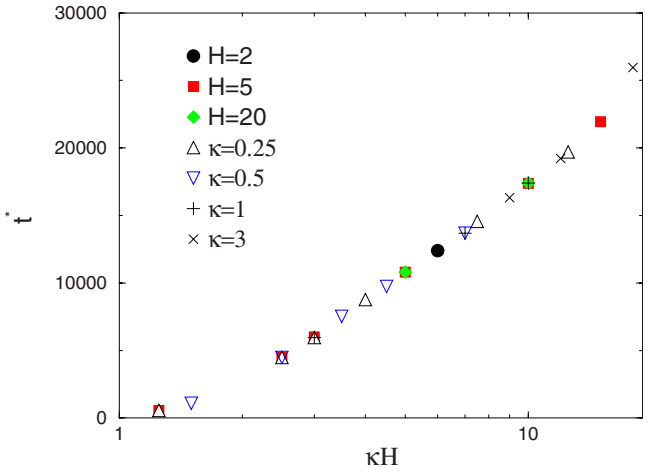

FIG. 9. (Color online) Linear-log plot of the simulation step at onset vs scaling variable κH, confirming Eq. (14). Legends indicate whether H or κ is kept fixed for the same symbol.

$$\xi^* \equiv \xi(t^*) = \frac{1}{2}\xi_0\kappa H. \tag{16}$$

Naturally, larger fragments are anticipated for thicker layers (see Sec. III G), independently of system sizes.

The absence of a solution to the equation $\kappa F_s(t)=s_{\max}(t)$ for $L<\xi_0\kappa H$ may be interpreted in two ways: (i) for fixed κ and H, there exists a critical system size

$$L_c(\kappa,H) \equiv \xi_0\kappa H, \tag{17}$$

below which the system never cracks. For $L>L_c$, L_c is nothing but $2\xi^*$, the correlation length at the onset. Alternatively, (ii) for fixed system size L, a thick layer does not crack if $\kappa H>L/\xi_0$. These agree with the basic experimental observations that a sufficiently small or thick layer does not crack but merely contracts.

The combination of κH in Eq. (14) implies that having a less frictional substrate has the same effect as having a greater thickness. Therefore, two identically prepared systems with different κ and H but the same product not only have the same history up to fracture, but they also fracture at the same time. Although thereafter the two systems behave differently due to explicit H dependence in the cracking criterion, it remains a useful characterization, as can be seen in Fig. 10. Thus, despite the intervening fragmentation process, the correlations at the onset have a strong persistence in the

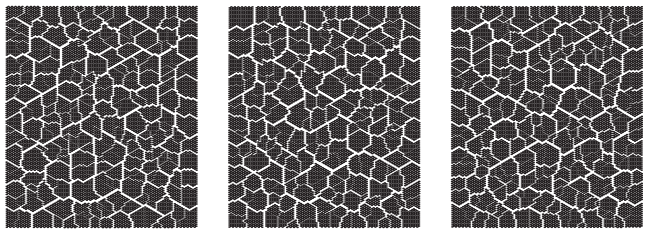

FIG. 10. Statistically similar final configurations at various combinations of κ and H with equal κH: from left to right, $(\kappa,H)=(0.25,10),(0.5,5),(1.25,2)$.

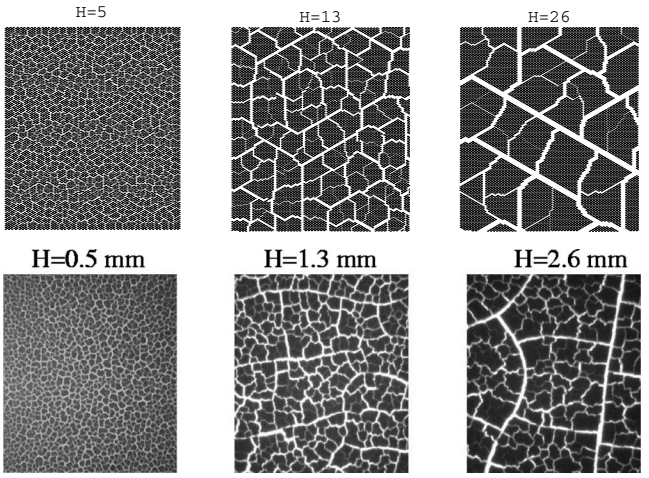

FIG. 11. Stationary patterns at different thickness H. Upper row: by simulation, $L=100$, $s=0.1$, $\kappa=0.25$ (increasing κ at fixed H has the same effect). Bottom row: from desiccation experiment of starch-water mixture with thickness matching that of simulation.

final fragmented state. Experimentally, this complementarity of the substrate and thickness is difficult to verify because κ is not easy to measure, but the predicted trend indeed agrees qualitatively with observations [39].

D. Morphology of crack networks

The difference in correlations also has an effect on the morphology of cracks. For very small κH, the substrate is very frictional or the layer very thin. Pinning is so strong that cracking events are highly localized. In a virtually uncorrelated stress environment, random nucleation of cracks soon appear (as t^* is small) but they do not propagate. Fragmentation is largely due to the percolation of independent microcracks. For $\kappa H \ll 1$, most bonds are ultimately broken and the system turns trivially into "powder" (i.e., isolated blocks in our context).

Going up in κH, the smaller friction or larger thickness allows stronger correlations up to fracture, as given in Eq. (16). Stress relaxation around crack tips becomes more effective, leading to more pronounced stress concentration and longer straight-crack segments. The resulting fragmentation process is hierarchical (see Fig. 2): after the primary straight cracks divide the system into a cellular network, secondary cracks break the large fragments into smaller ones, and so on [40,41]. Cracks of later generations are more "diffusive" in appearance because they tend to wiggle and branch due to diminishing stresses [42] and more pronounced screening from newly created free boundaries. The typical length of straight cracks between two joints is determined by the competition between stress concentration at crack tips that favors propagation, and pinning effect by the substrate that favors turning and branching. Since a larger κ or H enhances the former and suppress the latter, longer straight cracks are expected for larger κH. These features are shown in Fig. 11. At long times, fragmentation is complete, resulting in stationary fragments with areas that fit a log-normal distribution (cf. [28]), and a mean area $A \sim H^2$ (see below).

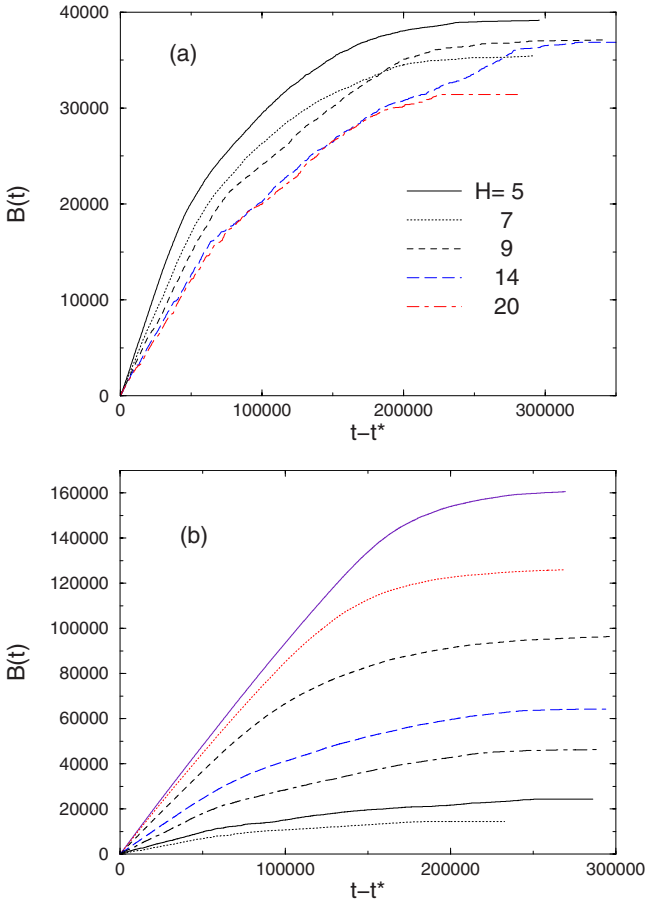

FIG. 12. (Color online) Typical plots of the number of broken bonds: $L=100$, $s=0.1$, FBC, (a) for fixed $\kappa=0.5$, different H; and (b) for fixed $H=10$, different $\kappa=0.12$, 0.15, 0.2, 0.3, 0.4, 0.7, and 1 from top to bottom. Note the crossover from linear growth to exponential saturation especially at large H in (a).

Experimentally, morphology may be characterized by the distribution $P(\theta)$ of crack angle θ at a joint. A shift of the peak position from $\theta \approx 90°$ to 60° as thickness decreases has been observed in amorphous media [39]. Although the usefulness of $P(\theta)$ in our model is limited by lattice anisotropies, we observed a shift from three peaks at $\theta=\pi$, $\pi/3$, and $2\pi/3$ to one peak at $\theta=\pi/3$ as κH was decreased. This corresponds to the shift from cracks terminating on encountering pre-existing ones to the case of a symmetric branching. A visual comparison with experimental configurations (Fig. 11) produced by slow desiccation of a starch-water mixture [11,43] reveals striking similarities. Such a qualitative change is also evident in the following variables.

E. Number of broken bonds

Starting from $t=t^*$, the total number of broken bonds $B(t)$ (i.e., area of cracked surfaces in experiments) increases monotonically. Figure 12 displays $B(t)$ for different combinations of κ and H. Two regimes, a linear one at early time and a subsequent exponential saturation, can be identified from those plots [44]. Matching with the configurations, we found that the linear behavior was associated with the propa-

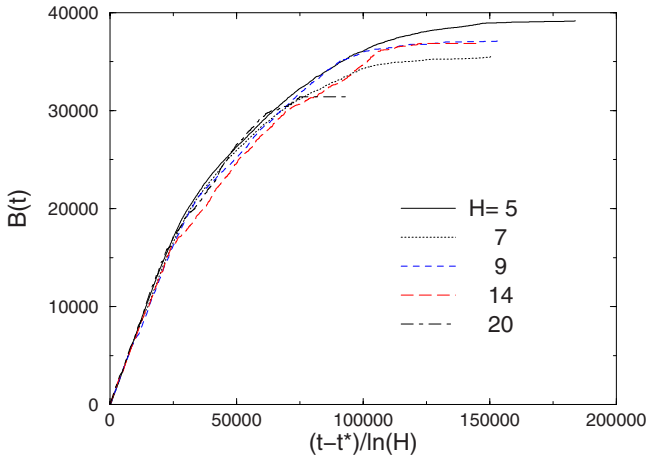

FIG. 13. (Color online) Scaling plot of the data in Fig. 12(a), showing the stretching of t by $\ln H$. $L=100$, $s=0.1$, $\kappa=0.5$, various H, FBC.

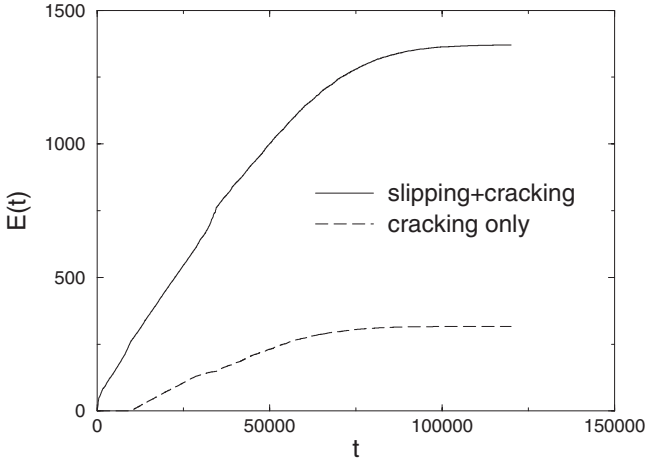

FIG. 14. Cumulative energy release due to slipping and cracking combined (upper curve) and due to cracking alone (lower curve). $L=100$, $s=0.1$, $\kappa=0.5$, $H=9$, corresponding to the evolution in Fig. 2. The kink near $t=34\,000$ signals the rupture of the system.

gation of primary straight cracks, the exponential behavior associated with late-stage diffusive cracks, and the crossover associated with a global rupture.

Since our rule limits at most one bond breaking per bundle per time step (see Sec. II), and that consecutive bond breakings within one time step are very rare, the growth rate of $B(t)$ is smaller than one. Due to relaxations for the elastic deformation around crack tips by slippings, during which time advances without bond breaking, the maximum rate is not attained. For larger H, the cracks are sparse, there are more relaxation events between bond breakings, and the growth rate is smaller as shown in Fig. 12(a). The detailed dependence on H is thus a complicated function of the frequency of relaxation events which in turn depends on the crack morphology. Empirically, the growth rate of B in the linear regime is found to scales as $(t-t^*)/\ln H$, as shown in Fig. 13. We do not yet have a simple argument for that $\ln H$ behavior. After the linear growth, fragmentation by straight cracks extensively modifies the stress field. The linear growth is over and the $\ln H$ scaling breaks down; crack growth becomes more random and diffusive. Being more random, the growth rate $dB(t)/dt$ is basically controlled by the number of existing unbroken bonds constant$-B(t)$, giving rise to an exponential approach to saturation.

F. Statistics of energy releases

Besides the number of broken bonds, energy release is also customarily monitored as for example by acoustic emission measurement. In our model, we calculated the total elastic energy $U(t)$ from the instantaneous positions of the blocks. The energy change associated with a broken bond is simply $\sigma^2/2$ where σ denotes the tension before breaking. In a slip, if all connecting bundles have the same coupling H, the energy dissipated by friction can be shown to be $\alpha F^2/2H$, where F is the force on the block before slipping, and $\alpha=1/3(1+s)$ (see Appendix). If some bundles are damaged (i.e., with some broken bonds), no general expression can be written down. But since broken or damaged bundles are relatively few $[B(t=\infty)\ll L^2]$, to a good approximation the energy release during an event of C bond breakages and S block slips can be expressed as $\varepsilon=\varepsilon_c+\varepsilon_s$, where

$$\varepsilon_c=\sum_{n=1}^{C}\frac{\sigma_n^2}{2}\approx\frac{C\kappa^2F_s^2}{2}, \tag{18}$$

$$\varepsilon_s\approx\sum_{m=1}^{S}\frac{\alpha F_m^2}{2H}\approx\frac{S\alpha F_s^2}{2H}. \tag{19}$$

Note that C is just dB/dt.

Figure 14 shows the cumulative change $E(t)\equiv U(0)-U(t)$, where $U(0)$ is the initial total elastic energy. Again we find a distinctive linear growth and an exponential saturation. They appear clearly in the energy release per event $\varepsilon(t)$ as a plateau and an exponential, as shown in Fig. 15(a). This figure also displays the independence of the linear growth rate of $E(t)$ with respect to L before the primary cracks reach the boundaries, but the extent of that regime increases as L^2. The exponential decay rate also scales as L^2, hence good data collapse can be obtained by plotting $\varepsilon(t)$ vs t/L^2 as in Fig. 15(b). On the other hand, for fixed L, both the linear growth rate and the decay rate are independent of H but the extent of the linear regime scales as $\ln H$. These results are exhibited in Fig. 16.

One can get some feeling for the role that friction plays by examining the fraction of energy release due to cracking alone, $\varepsilon_c/\varepsilon$. Typically, although $\varepsilon_c/\varepsilon$ can be quite large, clustering around 0.3–0.5 for the propagating-crack regime (see Fig. 17), the cumulative amount is much less (see Fig. 14) because the majority events consist of slippings only. Energy dissipated by friction, absent in a free-standing layer such as that considered by Griffith [23]), is unavailable to propagate cracks. In other words, running cracks are stabilized and arrested by the substrate.

Typical distributions of energy release $P(\varepsilon)$ are shown in Fig. 18. In view of the criticality in the precracking phase, we would expect to see a power law in $P(\varepsilon_s)$. That turns out not to be the case. The reason for the difference is that, in our

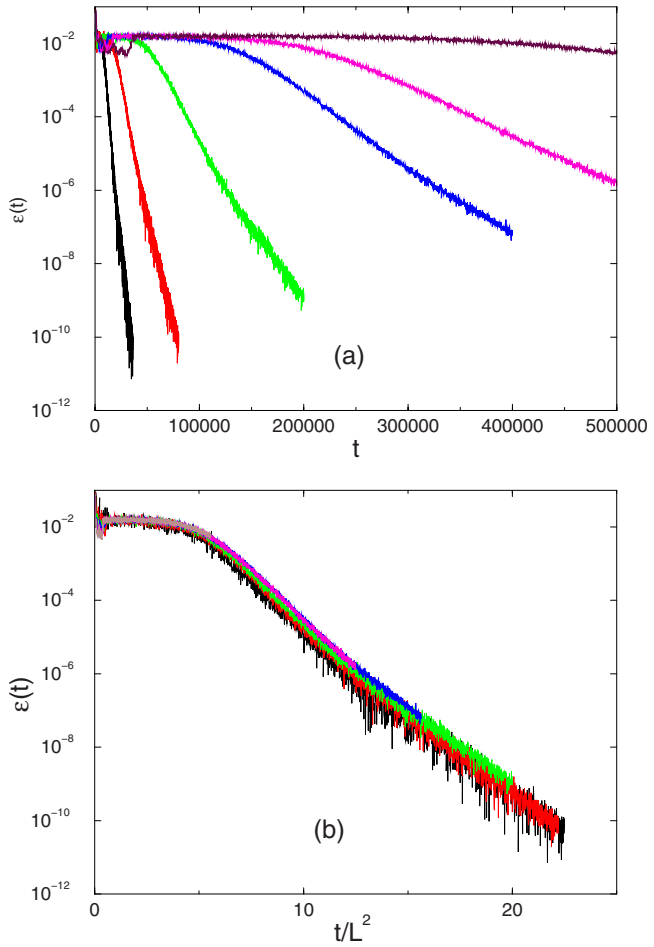

FIG. 15. (Color online) (a) Energy release per simulation step vs simulation step for different system size $L=40$, 60, 100, 160, 200, and 300 from left to right. $s=0.1$, $\kappa=0.5$, $H=5$ and FBC. (b) Scaling plot of the same data to show decay rate $\propto L^2$.

model, the stress decreases in time rather than being sustained. Hence it depicts an approach to equilibrium rather than a nonequilibrium steady state. This leads to energy release that diminishes in time. Such a difference, however, can be reconciled by a rescaling. The rescaled energy $\varepsilon_s/F_s^2 \propto S$ then duly exhibits the same power law as that for the slip size distribution. Roughly speaking, by dividing out $F_s(t)$ we remove the "approach-to-equilibrium" aspect of the dynamics so that the underlying power law in the stick-slip mechanism is revealed [45].

G. Scaling of the fragment size

Since fragment sizes can readily be determined in experiment, it is useful to examine the stationary fragment-size statistics as a test of the model. In particular, we are interested in the influences of the thickness and substrate property, and the mechanism by which the final scale is selected. As discussed above, the correlation of the stress field increases with κH and has a direct influence on the resulting fragment sizes. Given that a system of size $L > L_c$ cracks, the remaining question is when fragmentation will stop. We do not have a rigorous answer as the dynamics of interacting

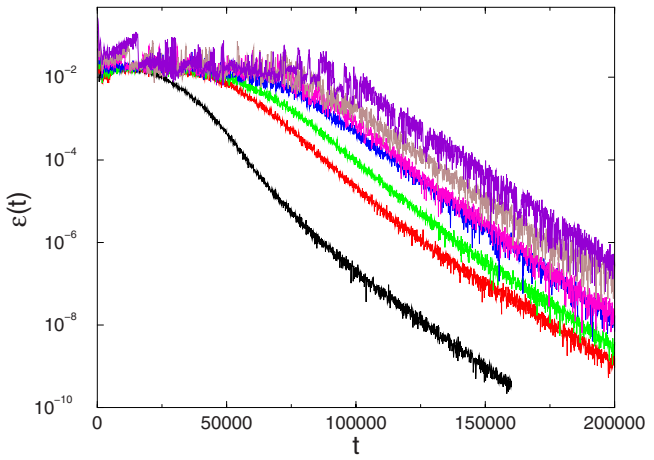

FIG. 16. (Color online) Effect of thickness in energy release per step. $H=3$, 5, 6, 8, 10, 12, and 17 from left to right, and $s=0.1$, $\kappa=0.5$ and FBC. The transient behavior at early times corresponds to the buildup of correlations prior to cracking.

cracks is highly nonlinear and complex. Intuitively, we expect fragmentation to stop when the typical fragment size decreases to a scale $\sim L_c$. It is a reasonable expectation in view of Eq. (17), i.e., that beyond that point the threshold simply does not decrease fast enough to catch the fall of the maximum stress so that no more bond will be broken. This argument predicts the scaling of the average fragment area

$$A(\kappa,H) \sim L_c^2 \propto (\kappa H)^2, \tag{20}$$

in complete agreement with measurements (Fig. 19). Experimentally the fragment area was also found to scale with the thickness square [39,46]. Our argument above implies the memory of the correlations at t^* persists in the fragmented state at $t=\infty$, reminiscent of similar generation of quenched disorder in systems governed by metastability and frustration

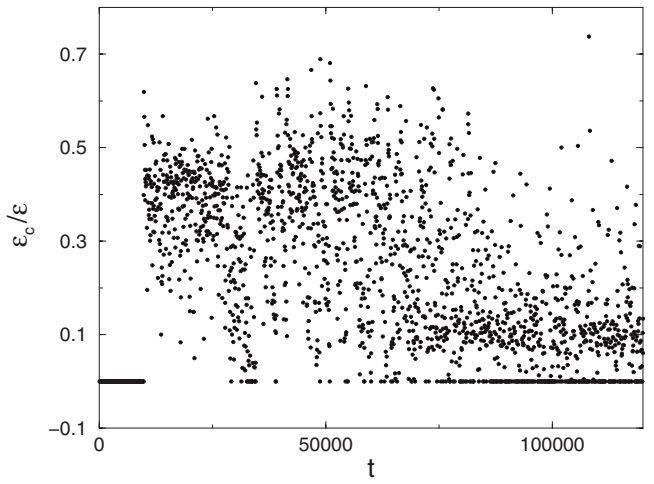

FIG. 17. The fraction of the energy released by cracking at each event. $L=100$, $s=0.1$, $\kappa=0.5$, $H=9$, and FBC, as in Fig. 2. $\varepsilon_c/\varepsilon=0$ for events without cracking. It clusters around 0.3–0.5 for the straight-crack regime and drops to 0.1 for the diffusive crack regime.

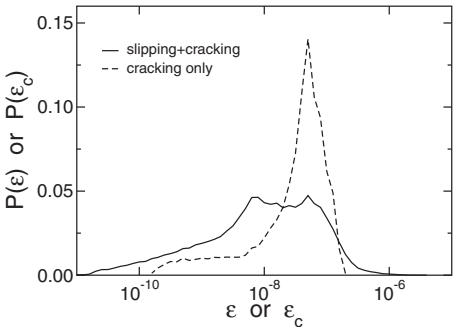

FIG. 18. Normalized distributions of energy release per simulation step for crackings and slippings combined $[P(\varepsilon)]$, and for cracking alone $[P(\varepsilon_c)]$, from one run, corresponding to the evolution in Fig. 2.

[47]—two features also central to the mechanism of surface fracture here.

IV. CONCLUSION AND OUTLOOK

Motivated by desiccation experiments, we carried out a thorough study of a bundle-block model for the aspects of pattern formation and selection of cracks in in-plane fracture induced by a quasistatic driving. In developing the model, our priority was physical relevance and consistency with experiments, as well as simplicity with a small set of control parameters. Fairly comprehensive theoretical understanding can be achieved. In this work, we focused on elucidating the effects of substrate, sample thickness and system size on measurable quantities. Those effects were found to be complementary in the sense that it is the product of the parameters that characterizes the statistics of the dynamics and patterns. By exploiting metastability and energy balance, we have shown analytically and numerically how self-organization in the stress field dictates the properties of the fractured state, especially the final fragment size. Our results answer, at least qualitatively, why thin layers crack finely and thick ones are hard to crack, and why geometrical similarities exist over wide range of scales. Judging from agreement with experimental observations, the model appears to capture many salient features of real systems. Despite the specific implementation, there is the general idea that stick-slip generates correlations in the strain field, which in turn dictate crack growth and determine fragment sizes. We expect the idea to apply to similar situations governed by stick-slip mechanisms.

ACKNOWLEDGMENTS

The authors would like to thank Yves Brechet, K.-w. To, and C.K. Chan for useful discussions at early stages of this work. This work is partially supported by the National Science Council of R.O.C. and a Romanian IDEI/PN2 nr. 236 research grant.

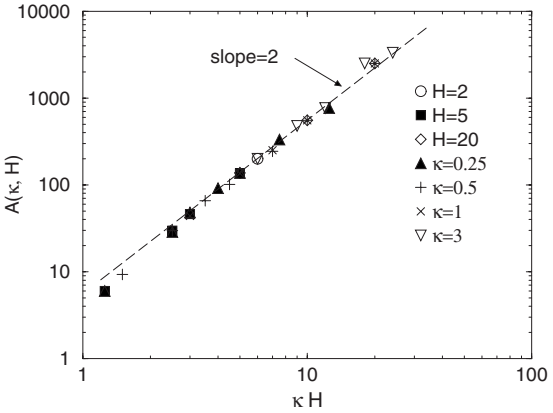

FIG. 19. Scaling of mean fragment area A in thickness and substrate property via scaling variable κH. $L=100$, $s=0.1$, with either fixed κ or H as indicated.

APPENDIX: SLIP DISTANCE

First consider the case of zero kinetic friction. Suppose the block (i,j) slips by $\delta\vec{r}=(\delta x,\delta y)$. From Eq. (3), the force is changed,

$$F_x \to 0 = F_x - \delta x \sum_{i=1}^{6} (sS_i^2 + C_i^2)H_i - \delta y \sum_{i=1}^{6} (1-s)C_iS_iH_i; \tag{A1}$$

$$F_y \to 0 = F_y - \delta x \sum_{i=1}^{6} (1-s)S_iC_iH_i - \delta y \sum_{i=1}^{6} (sC_i^2 + S_i^2)H_i. \tag{A2}$$

This gives the slip distance linear in the forces,

$$\delta x = \frac{CF_x - BF_y}{AC - B^2}; \quad \delta y = \frac{-BF_x + AF_y}{AC - B^2}, \tag{A3}$$

where $A=\Sigma_{i=1}^{6}H_i(sS_i^2+C_i^2)$, $B=\Sigma_{i=1}^{6}H_i(1-s)C_iS_i$, and $C=\Sigma_{i=1}^{6}H_i(sC_i^2+S_i^2)$. If all bonds are intact, as is the case in phase I of the evolution discussed in Sec. III, B vanishes by symmetry and we get

$$\delta x = \frac{\alpha F_x}{H}; \quad \delta y = \frac{\alpha F_y}{H}; \tag{A4}$$

hence $\delta r \equiv \sqrt{(\delta x)^2+(\delta y)^2} = \alpha F/H$, where $\alpha = 1/3(1+s)$ for the triangular lattice [36]. The energy dissipated by friction is given by $\int_0^{\delta r} F(r)dr = \alpha F^2/2H$.

Next, we consider the more general case of nonzero kinetic friction. There is then an additional threshold F_k, where $0<F_k<F_s$. A slipping block is arrested when the net force from its neighbors drops below F_k. The consequence of a slip is modified simply: $F_x \to F_kF_x/F$ and $F_y \to F_kF_y/F$. We obtain the same results as above except that F_x and F_y are now replaced by $F_x(1-F_k/F)$ and $F_y(1-F_k/F)$, respectively. The evolution of the model is the same except that the slipping distances are smaller by the factor $1-F_k/F$, which is essentially $1-F_k/F_s$, and so is the energy dissipation.

[1] P. S. Stevens, *Patterns in Nature* (Atlantic Monthly Press, Boston-Toronto, 1974).

[2] J. P. Gollub and J. S. Langer, Rev. Mod. Phys. **71**, S396 (1999).

[3] M. C. Cross and P. C. Hohenberg, Rev. Mod. Phys. **65**, 851 (1993).

[4] *Pattern Formation in Complex Dissipative Systems: Fluid Patterns, Liquid Crystals, Chemical Reactions*, edited by S. Kai (World Scientific, Singapore, 1992).

[5] B. Lawn, *Fracture of brittle solids*, 2nd ed. (Cambridge University Press, Cambridge, England, 1993).

[6] W. B. Lang, Science **98**, 583 (1943); J. T. Neal, A. M. Langer, and P. F. Kerr, Geol. Soc. Am. Bull. **79**, 69 (1968).

[7] J. Walker, Sci. Am. **255**, 204 (1986).

[8] P. Meakin, Thin Solid Films **151**, 165 (1987); A. T. Skjeltorp and P. Meakin, Nature (London) **335**, 424 (1988).

[9] D. Hull and B. D. Caddock, J. Mater. Sci. **34**, 5707 (1999).

[10] K. A. Shorlin, J. R. de Bruyn, M. Graham, and S. W. Morris, Phys. Rev. E **61**, 6950 (2000).

[11] T. Mizuguchi, A. Nishimoto, S. Kitsunezaki, Y. Yamazaki, and I. Aoki, Phys. Rev. E **71**, 056122 (2005).

[12] A. Nakahara and Y. Matsuo, Phys. Rev. E **74**, 045102 (2006).

[13] K. B. Singh and M. S. Tirumkudulu, Phys. Rev. Lett. **98**, 218302 (2007).

[14] L. Goehring, Phys. Rev. E **80**, 036116 (2009).

[15] J. E. Gordon, *The New Science of Strong Materials, or Why you Don't Fall Through the Floor*, 2nd ed. (Penguin, Harnondsworth, 1976).

[16] M. Marder and J. Fineberg, Phys. Today **49** (9), 24 (1996).

[17] E. S. C. Ching, J. S. Langer, and H. Nakanishi, Phys. Rev. Lett. **76**, 1087 (1996); J. S. Langer and A. E. Lobkovsky, J. Mech. Phys. Solids **46**, 1521 (1998).

[18] M. Kachanov, Adv. Appl. Mech. **30**, 259 (1993).

[19] S. Kitsunezaki, Phys. Rev. E **60**, 6449 (1999).

[20] Y. Cohen, J. Mathiesen, and I. Procaccia, Phys. Rev. E **79**, 046109 (2009).

[21] *Statistical Models for the Fracture of Disordered Media*, edited by H. J. Herrmann and S. Roux (North-Holland, Amsterdam, 1990).

[22] L. Golubović and S. Feng, Phys. Rev. A **43**, 5223 (1991).

[23] A. A. Griffith, Philos. Trans. R. Soc. London, Ser. A **221**, 163 (1921).

[24] J. D. Gunton, M. San Miguel, and P. S. Sahni, in *Phase Transitions and Critical Phenomena*, edited by C. Domb and J. L. Lebowitz (Academic, New York, 1983), Vol. 8, p. 267.

[25] L. de Arcangelis, S. Redner, and H. J. Herrmann, J. Phys. (France) Lett. **46**, 585 (1985).

[26] T. Hornig, I. M. Sokolov, and A. Blumen, Phys. Rev. E **54**, 4293 (1996).

[27] K. M. Crosby and R. M. Bradley, Phys. Rev. E **55**, 6084 (1997); Philos. Mag. B **76**, 91 (1997).

[28] K.-t. Leung and J. V. Andersen, EPL **38**, 589 (1997); J. V. Andersen, D. Sornette, and K.-t. Leung, Phys. Rev. Lett. **78**, 2140 (1997).

[29] K.-t. Leung and Z. Néda, Phys. Rev. Lett. **85**, 662 (2000).

[30] Phani Kumar V. V. Nukala, S. Zapperi, and S. Simunovic, Phys. Rev. E **71**, 066106 (2005).

[31] J. W. Hutchinson, Adv. Appl. Mech. **29**, 63 (1991).

[32] Apart from simplicity, another reason for our choice is that if the thresholds are allowed to vary independently, a stationary, nontrivial pattern may not exist unless parameters are fine tuned [28]. Since no such tuning is evident in nature, we choose to fix the ratio of the two thresholds.

[33] Subject to $O(1/L)$ boundary corrections in FBC.

[34] The algorithm is non-Abelian: the configurations depend on the detailed order of slippings and crackings, but the statistics do not. Nevertheless, random order of updating is used to eliminate any systematic dependence.

[35] Partially and fully periodic boundary conditions lead to similar patterns with the same fragment-area statistics.

[36] α specifies the fraction of the force components distributed to neighbors in a slip. It is $1/2(1+s)$ for square lattices. Note that in our model, all force components are strictly conserved locally during slipping *and* cracking for any s.

[37] P. Bak, C. Tang, and K. Wiesenfeld, Phys. Rev. A **38**, 364 (1988).

[38] K.-t. Leung, J. V. Andersen, and D. Sornette, Phys. Rev. Lett. **80**, 1916 (1998); Physica A **254**, 85 (1998).

[39] A. Groisman and E. Kaplan, EPL **25**, 415 (1994).

[40] S. Bohn, J. Platkiewicz, B. Andreotti, M. Adda-Bedia, and Y. Couder, Phys. Rev. E **71**, 046215 (2005).

[41] K. B. Toga and B. E. Alaca, Phys. Rev. E **74**, 021405 (2006).

[42] We have checked that smaller prestrain s results in more wiggling and branching cracks, and the typical length of straight-crack segments increases with s.

[43] Z. Neda and K.-t. Leung (unpublished).

[44] For sufficiently large L and κH, distinct linear regions exist corresponding to successive generations of straight cracks. Two such generations are evident in Fig. 12 for $\kappa=0.5$, $H=14$ and $H=20$.

[45] An analogous situation is found in the display of SOC in systems approaching equilibrium [38].

[46] Y. Bréchet, D. Bellet, and Z. NédaSolid State Phenomena **42-43**, 247 (1995).

[47] J. P. Bouchaud and M. Mezard, J. Phys. I **4**, 1109 (1994); S. Boettcher and M. Paczuski, Phys. Rev. Lett. **79**, 889 (1997).